Letters

A Low-Cost DC Chopper With Coupling Transformer for Offshore Wind VSC-HVdc System

Lei Qi, Sihang Wu, Xiangyu Zhang, Meng Zhang, Chengzhu Liu, Hongbin Wang, and Long Wu

***Abstract*—The dc chopper (DCC) is the key equipment of offshore wind voltage source converter based high-voltage direct current (VSC-HVdc) system. Combining the advantages of the ac chopper and the centralized DCC, a novel dc chopper with coupling transformer (CT-DCC) is proposed. The use of the coupling transformer can reduce the voltage on the concentrated resistor to eliminate the high-voltage wall bushing effectively. Compared with the traditional DCC, the cost of CT-DCC is reduced by 35% for ±400 kV/1100 MW offshore wind VSC-HVdc project. In addition, the application of the coupling transformer provides an opportunity for the introduction of freewheeling inductance, which greatly eliminates the interference of pulse-current generated by the existing DCC on dc-link voltage. Through system simulation, the peak value of the dc-link voltage during the fault ride through is 1.02 p.u., and the dc-link voltage ripple is only 1%–2%, which meets the system requirements. After the detailed analysis of the working principle and characteristics of CT-DCC, the control strategy and design principle are given. Furthermore, a prototype experiment of up to 10 kV/10 MW is conducted to verify the feasibility of CT-DCC.**

***Index Terms*—Coupling transformer, dc chopper (DCC), offshore wind voltage source converter based high-voltage direct current (VSC-HVdc) system.**

I. Introduction

With the rapid development of offshore wind system, the voltage source converter based high-voltage direct current (VSC-HVdc) transmission technology has a very broad application prospect [1]. Fig. 1 presents the schematic diagram of China's first and largest offshore wind VSC-HVdc project (±400 kV/1100 MW).

Offshore wind farms are connected by VSC-HVdc system. When a short-circuit fault occurs at the ac side of the onshore converter station, the ac voltage's drop will lead to the decrease of the power delivery capacity of the VSC-HVdc system, whereas the power generated by the wind farm will not change in a short time, causing the power imbalance of the offshore wind power delivery system. And the excess power will continue to charge the capacitor of the VSC-HVdc system, resulting in the dc-link voltage exceed 1.1 p.u. in about 30 ms [2], [3]. In order to ensure that the dc-link voltage is below the limit voltage, the surplus power must be dissipated or the power generated by offshore wind farms must be reduced. Otherwise, dc-link overvoltage will damage the converter and other equipment, threatening the safe and stable operation of the system [4]. Therefore, it is of great significance to realize the fault ride through (FRT) of offshore wind VSC-HVdc system. The existing research solutions for FRT can be summarized in two ways. The first is to control the wind turbine to actively reduce the output power through fast communication method, frequency up method or voltage down method to maintain the system power balance [5], [6], and the second is to use energy dissipation equipment to absorb surplus power. Because the reliability of the wind turbine and the delay of signal transmission will increase the possibility of system FRT failure, a chopper circuit with an energy dissipation resistor is usually added to dynamically absorb excess power [7].

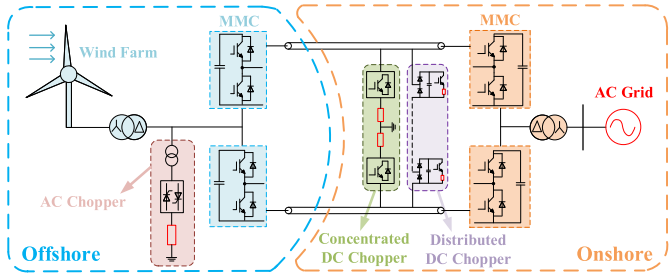

Fig. 1. Schematic diagram of ±400 kV/1100 MW offshore wind VSC-HVdc project.

As shown in Fig. 1, the installation of energy dissipation equipment is located inside the wind turbine, at the outlet side of the offshore ac transformer and at the onshore dc bus side at present. However, the energy dissipation equipment located inside the wind turbine is generally used as backup protection due to its limited absorbed power and high action delay [4], [8]. The chopper circuit is mainly divided into two types, namely,

Manuscript received August 31, 2021; revised November 1, 2021 and November 27, 2021; accepted December 10, 2021. Date of publication December 14, 2021; date of current version January 19, 2022. This work was supported in part by the Natural Science Foundation Project of China under Contract 52107004 and in part by the Postdoctoral Science Foundation of China under Contracts 2020M680484 and 2021T140201. *(Corresponding author: Xiangyu Zhang.)*

Lei Qi, Sihang Wu, and Xiangyu Zhang are with the State Key Laboratory of Alternate Electrical Power System With Renewable Energy Sources, North China Electric Power University, Beijing 102206, China (e-mail: qilei@ncepu.edu.cn; 13261687255@163.com; zhangxiangyu11@gmail.com).

Meng Zhang, Chengzhu Liu, Hongbin Wang, and Long Wu are with Beijing Power Equipment General Factory Co., Ltd., Beijing 102401, China (e-mail: magic.meng@163.com; liuchengzhu@bpeg.cn; 601382427@qq.com; wulongchp@126.com).

Color versions of one or more figures in this article are available at https://doi.org/10.1109/TPEL.2021.3135286.

Digital Object Identifier 10.1109/TPEL.2021.3135286

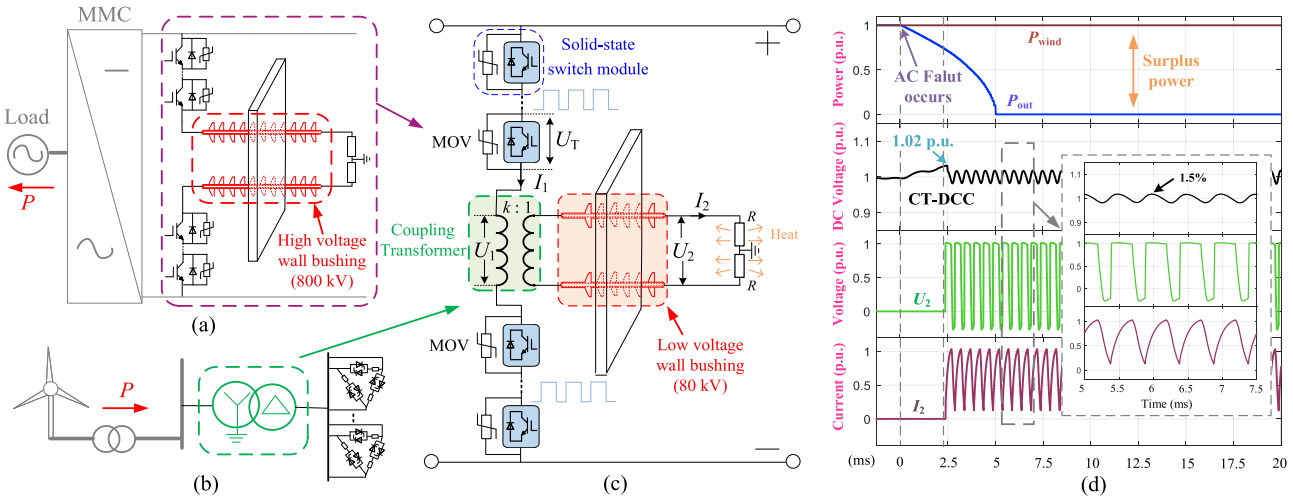

Fig. 2. Proposed CT-DCC. (a) Concentrated DCC. (b) ACC. (c) Proposed CT-DCC. (d) Operating analysis of CT-DCC.

the ac chopper (ACC) and the dc chopper (DCC). ACC is located at the offshore ac side. It reduces the voltage through the transformer and then uses the thyristor to control the resistor to dissipate the excess power. Compared with DCC, ACC cannot dynamically adjust the dissipated power and must be installed offshore, which adds extra volume and weight, causing the high cost of the offshore converter platform [9]. Hence, DCC is a better choice for the offshore wind system to dissipate surplus power.

At present, there is only a small amount of literature on DCC. The typical structure of DCC can be divided into two types, centralized DCC and distributed DCC, as presented in Fig. 1. The centralized DCC replaces the thyristor in ACC through the series-connected solid-state switch modules, and realizes the continuously adjustable power dissipation capacity by changing the duty cycle [10]. Because the centralized DCC adopts pulse-width modulation, the pulse-current flows through the concentrated resistor, making the large fluctuation on the dc-link voltage. In order to overcome the problem of large dc-link voltage ripple, a distributed DCC is proposed in [11]. It is composed of several energy dissipation modules in series. However, in order to avoid the influence of the heat generated by the resistor on the power devices, the heat dissipation of the resistor should be considered in DCC. The resistor of centralized DCC can be arranged outdoors through high-voltage wall bushing, which is no need to consider the heat dissipation, but the resistor of distributed DCC must be placed inside each module, which is close to the power device, so the water-cooling system is needed. In addition, since the energy dissipation resistor placed outdoors has no temperature limit, it has advantages over the resistor placed inside the valve hall in terms of safety, reliability, and cost.

A centralized DCC with coupling transformer (CT-DCC) is proposed to overcome the defects of the existing DCC. The combination of centralized DCC and ACC provides a low-cost and low-disturbance scheme for FRT. This letter first introduces the topology and working principle of CT-DCC. The characteristics of CT-DCC are discussed in detail after system analysis, and the control strategy and design principle are given. Furthermore, a prototype experiment of up to 10 kV/10 MW is conducted to verify the feasibility of the proposed CT-DCC.

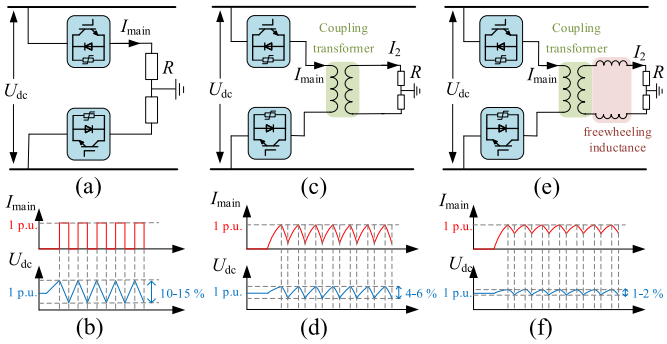

Fig. 3. Principle of CT-DCC. (a) Existing DCC topology. (b) FRT of existing DCC. (c) CT-DCC topology. (d) FRT of CT-DCC. (e) CT-DCC with freewheeling inductance topology. (f) FRT of CT-DCC with freewheeling inductance.

II. Proposed CT-DCC

A. Topology of the Proposed CT-DCC

The existing DCC is shown in Fig. 2(a), and the solid-state switch modules are connected in series with the centralized resistor. Solid-state switch modules include the metal oxide varistors (MOVs) to protect switch modules [7]. However, the existing DCC needs high-voltage wall bushing, and the cost is very high (accounts for 40%–60% of the total DCC cost). With the increase of voltage level, the cost of wall bushing will rise sharply, and the requirement of reliability is more difficult to realize in technology. Through the investigation of relevant manufacturers, when the voltage level is from 80 to 800 kV, the cost is increased by 15 times. Moreover, the high dc-link voltage ripple (up to 10%) may affect the control and protection strategy of the system shown in Fig. 3(a) and (b). ACC, as shown in Fig. 2(b), adopts the scheme of the transformer connected with thyristors, and puts resistors into groups to dissipate power. It has the advantages of simple technology, but it covers a large area and is limited in the application of offshore wind project.

TABLE I
CT-DCC REQUIREMENTS FOR ±400 KV/1100 MW VSC-HVDC SYSTEM

Item	Value
System rated DC voltage and current	800 kV/1.375 kA
Power rating of CT-DCC	0-1100 MW adjustable
DC-link voltage ripple range	0.95-1.10 p.u.

TABLE II
CT-DCC PARAMETERS FOR ±400 KV/1100 MW VSC-HVDC SYSTEM

Item	Value
Operating frequency	50 Hz ~ 2 kHz
Solid-state power device (IGCT)	4.5 kV/2 kA
MOV	2.4 kV (at 1 mA) / 3.3 kV (at 3 kA) / 40 kJ
Ratio of coupling transformer	800 kV:80 kV
Freewheeling inductance	4 mH
Energy dissipation resistor (R)	5 Ω

TABLE III
COST COMPARISON OF ENERGY DISSIPATION SCHEMES

Item	Switches	Resistor	Wall bushing	Coupling transformer	Total
DCC	360 p.u.	90 p.u.	300 p.u.		750 p.u.
CT-DCC	360 p.u.	90 p.u.	20 p.u.	20 p.u.	490 p.u.

Combined with the advantages of centralized DCC and ACC, the proposed CT-DCC is shown in Fig. 2(c). Drawing on ACC's idea of using a transformer to reduce the voltage on the resistor, the coupling transformer is introduced on basis of the existing DCC, and the concentrated resistor (R) is arranged at the low-voltage side of the transformer to reduce the voltage level of wall bushing and greatly saves the cost. For ±400 kV/1100 MW system, the requirements and the parameters of CT-DCC are presented in Tables I and II, respectively, and the parameters design is analyzed in detail in Section III. Table III presents the cost comparison of different energy dissipation schemes. The cost of a single switch solid-state switch module is 1 p.u. Compared with the traditional DCC, the cost of CT-DCC is reduced by 35%. Moreover, the inductance of the coupling transformer itself will also reduce the current change rate and then reduce the voltage ripple to 4%–6%, as presented in Fig. 3(c) and (d).

Furthermore, using freewheeling inductance in the low voltage side of the coupling transformer can make the current continuous, overcoming the adverse effect of the existing DCC on dc-link voltage ($U_{\rm dc}$) greatly and improving the system stability. It can be seen from Fig. 3(e) and (f) that the dc-link voltage fluctuation caused by CT-DCC during the operation is only 1%–2%. Meanwhile, due to the use of inductance, the MOV will operate during the FRT, absorbing part of the surplus power, improving the utilization rate of the MOV.

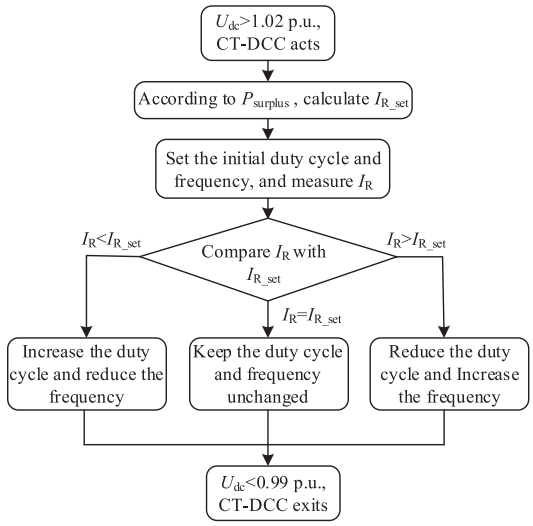

Fig. 4. Modulation strategy of CT-DCC.

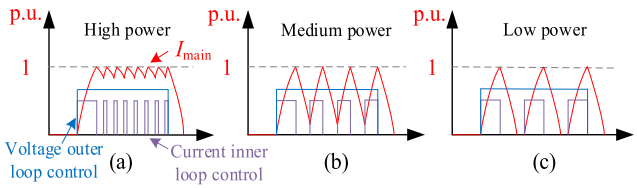

Fig. 5. Operation effect of CT-DCC under different working conditions. (a) Maximum power. (b) Medium power. (c) Minimum power.

B. Working Principle of the Proposed CT-DCC

The CT-DCC adopts voltage outer loop control and current inner loop control shown in Fig. 4. When the dc-link voltage ($U_{\rm dc}$) exceeds the set value (1.02 p.u.), CT-DCC is put into operation. At this time, the effective value of the current ($I_{R\_\rm set}$) flowing through the energy dissipation resistor is calculated according to the system surplus power ($P_{\rm surplus}$). Then, the initial frequency and duty cycle of CT-DCC are set. Based on the topology shown in Fig. 3(e), take the FRT process of ±400 kV/1100 MW system as an example, and the simulation results are shown in Fig. 2(d). The initial frequency is 2 kHz and the duty cycle is 50%. By measuring the current (I_R) flowing through the resistor, it is compared with the calculated results ($I_{R\_\rm set}$). When $I_{\rm R}$ is greater than $I_{R\_\rm set}$, the duty cycle is reduced and the frequency is increased. When I_R is less than $I_{R\_\rm set}$, the frequency is reduced and the duty cycle is increased. When they are equal, the frequency and duty cycle remain the same. The corresponding control and operation effects of CT-DCC under different working conditions are shown in Fig. 5.

When $U_{\rm dc}$ rises to CT-DCC stare value, the solid-state switch module is put into operation, the coupling transformer bears dc-link voltage, current of energy dissipation circuit (I_2) starts to rise and $U_{\rm dc}$ begins to fall. After the solid-state switch module turns OFF, the current at the primary side of the coupling transformer (I_1) changes little due to the freewheeling effect of the inductance. At this time, the current flowing through the switches becomes 0, and the current flowing through the

MOVs and I_1 are equal. When the current flowing through the MOVs is basically unchanged, the voltage of the MOV also remains unchanged. Because different MOVs have different *U–I* characteristics, taking the MOV used in solid-state switch module in practical engineering as an example, the voltage of the solid-state switch modules (U_T) will reach 1.3 p.u. at 2 kA. Since the dc-link voltage remains unchanged, the voltage at the primary side of the coupling transformer is –0.3 p.u. accordingly, and the voltage of the energy dissipation circuit (U_2) will change to 0.3 p.u. in reverse. After that, the above process is repeated continuously to stabilize the dc-link voltage near the rated value.

III. Characteristic Analysis of CT-DCC

A. Energy Dissipation Circuit

For different VSC-HVdc systems, CT-DCC should be designed according to the system requirements and its own operation characteristics. Through the analysis of CT-DCC action process, it can be known that the ratio of coupling transformer (k) not only directly affects the voltage level of wall bushing but also affects the parameter selection of concentrated resistor. It should be pointed out that if an iron core transformer is used, it will bear the alternating pulse voltage of positive and negative polarity in a short time, and the current reaches 10–20 kA, which may lead to the saturation of the iron core. Considering the above problems when designing the coupling transformer, this manuscript adopted the air core transformer in the final scheme. Although it has a high cost and large magnetic leakage compared with the iron core transformer, it will not have the problem of magnetic saturation and can realize the transformation of pulse voltage. The air core transformer is essentially an inductance, so it does not need to ensure bipolar balance. It should be noted that for CT-DCC, the transformer does not bear voltage and no current flows through it during normal operation. The current flows through it only after CT-DCC acts in case of fault. Therefore, surge current rather than rated current should be considered in the design of the transformer.

In addition, the use of freewheeling inductance changes the current characteristics of the energy dissipation circuit. The larger the inductance is, the smaller the fluctuation of the current and the disturbance of the dc-link voltage will be, but it will increase the energy absorbed by the MOVs. Thus, after considering the system requirements presented in Table I, economy and other factors, the parameters of coupling transformer and freewheeling inductance selected in this manuscript are listed in Table II.

As can be seen from Fig. 2(d), 4 mH inductance ensures continuous current and the voltage ripple range is 0.99–1.02 p.u. With the use of 800:80 kV coupling transformer, the cost of wall bushing is only 1/15 of that of the existing DCC. When the coupling transformer and freewheeling inductance are determined, the parameters of the concentrated resistor can be expressed by (1). The fixed resistor is lower than or equal to the equivalent resistor. After considering a certain engineering margin, it is selected as 5 Ω. As can be seen from the CT-DCC operation characteristics shown in Fig. 2(d), the instantaneous power of the resistor in the proposed CT-DCC topology is higher than that in the traditional DCC. But the FRT time of the two

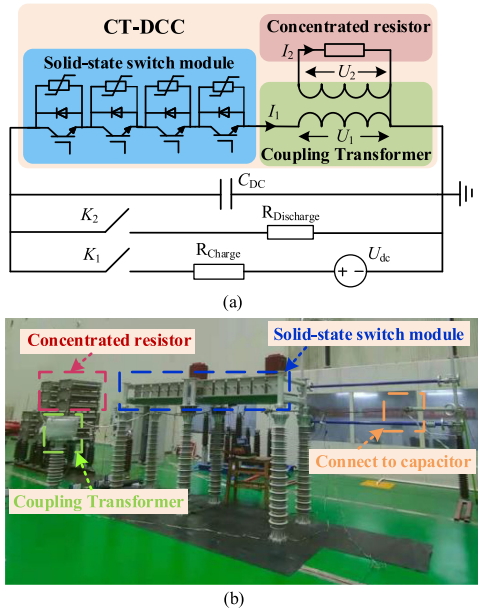

Fig. 6. Principle and arrangement of the CT-DCC experiment. (a) Experimental platform. (b) Experimental site layout.

schemes is the same, so the total energy absorbed by the energy dissipation resistor is the same. For the resistor in CT-DCC, on the one hand, it is placed outdoors and far away from the main electrical equipment in the valve hall, and the short-term heat dissipation will not affect the normal operation of the equipment in the valve hall. On the other hand, for the working condition of instantaneous action, the design and manufacture of the energy dissipation resistor only consider the total energy absorbed rather than the instantaneous power of the resistor. Moreover, the interval time between two faults is usually several hours, and there will be a long time for heat dissipation after the action of the energy dissipation resistor. Therefore, the low-voltage resistor in CT-DCC has advantages over the high-voltage resistor in the traditional DCC in cost and technology

$$R = P_{\text{wind}}/(kP_{\text{wind}}/U_{\text{dc}})^2. \tag{1}$$

B. Solid-State Switch Modules

The solid-state switch modules must turn ON and OFF continuously in the FRT. The operation frequency of 2 kHz of the switch module ensures that the temperature rise of the equipment is within the allowable range. During the turn-OFF process, the voltage threshold characteristic of MOV turns the overvoltage of the integrated gate commutated thyristor (IGCT) under breakdown voltage, and MOV begins to absorb energy. Since the peak voltage of IGCT is 4.5 kV, the residual voltage of MOV is designed to be 3.3 kV after considering the engineering margin. Due to the aging characteristics of MOV, it cannot exceed the rated voltage for a long time. Taking ±400 kV/1100 MW system as an example, 360 switch modules are connected in series at dc side, and the voltage of each module is below 2.4 kV.

For the CT-DCC, due to the use of air core transformer and freewheeling inductance, it is an inductive load. The MOV not only limits the overvoltage but also absorbs some energy in the

TABLE IV
COMPARISON OF DCC AND CT-DCC

Characteristics	DCC	CT-DCC
Component equipment	High voltage wall bushing, Solid-state switch module, High voltage resistor	Low voltage wall bushing, Solid-state switch module, Low voltage resistor, Coupling transformer, Freewheeling inductance
Control	Pulse width modulation according to DC-link voltage	Control of variable duty cycle and frequency according to DC-link voltage and resistor current
Operation effect	DC-link voltage ripple up to 10%	DC-link voltage ripple up to 1-2%

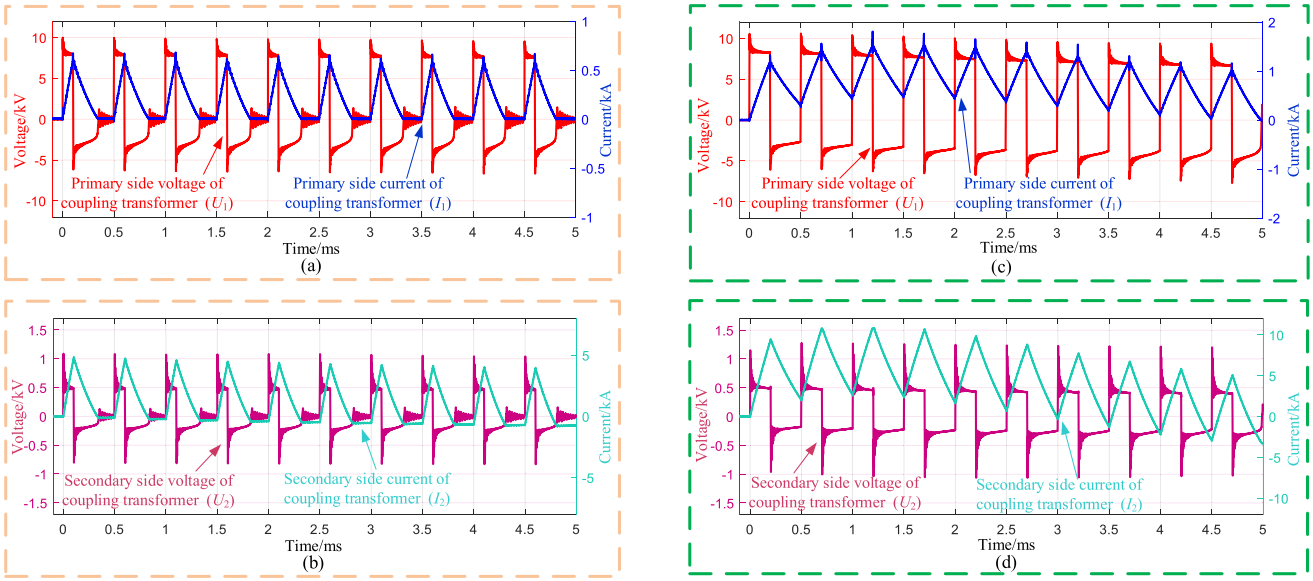

Fig. 7. Experimental results of CT-DCC. (a) Primary-side waveforms of CT-DCC at duty ratio = 20%. (b) Secondary-side waveforms of CT-DCC at duty ratio = 20%. (c) Primary-side waveforms of CT-DCC at duty ratio = 40%. (d) Secondary-side waveforms of CT-DCC at duty ratio = 40%.

FRT. Assuming that the operation frequency of CT-DCC is f and the single turn-OFF time of switch module is T_b, the maximum total energy absorbed by the MOV can be expressed as

$$E_{\max} = V_{\text{res}} \cdot I_b \cdot f \cdot T_b \tag{2}$$

where V_{res} is the residual voltage of MOV, I_b is the working current of CT-DCC, and $E_{\max}$ cannot exceed the maximum energy absorption limit of MOV.

For the use of MOVs, generally speaking, the time of one operation of CT-DCC is about 300–500 ms, and the interval time between two faults is up to several hours. Considering extreme working conditions, if the ac side fault of ±400 kV/1100 MW system lasts for 1 s, the total energy absorbed by the MOVs with 360 solid-state switch modules in parallel is 10.7 MJ according to the simulation results of Fig. 2(d). And the energy absorbed by a single MOV is 29 kJ, which is less than 40 kJ. Therefore, the short-term use of MOVs is acceptable in practice.

To sum up, Table IV presents the characteristics of the DCC and CT-DCC in detail. Compared with the traditional DCC, CT-DCC adds a coupling transformer and freewheeling inductance, which is complex in control. In addition, MOVs also absorb some energy, but these defects can be overcome. Moreover, CT-DCC reduces the voltage level of wall bushing and dc-link voltage ripple, which has great advantages in cost and performance.

TABLE V
EQUIVALENT EXPERIMENTAL PARAMETERS OF CT-DCC

Item	Value
Capacitor (C_{DC})	2 mF
Concentrated resistor	0.1 Ω
Ratio of coupling transformer	10 kV:1 kV
Primary / secondary inductance of coupling transformer	6 mH/60 μH

IV. EXPERIMENTAL VALIDATION

A. Development of a Prototype and Test Scheme for CT-DCC

A 10-kV/10-MW prototype of the CT-DCC is built to verify the effectiveness of the proposed CT-DCC. Fig. 6(a) and (b), respectively, shows the experimental principle of the CT-DCC prototype and the layout scheme of the experimental platform. Four solid-state switch modules are connected in series with the coupling transformer, and the energy dissipation resistor is arranged on the secondary side of the coupling transformer to form the CT-DCC prototype. In order to equalize the surplus power dissipated by CT-DCC during actual operation, the equipment parameters are presented in Table V. The capacitor is precharged to 10 kV. The CT-DCC works at an adjustable frequency and duty cycle, whereas the energy of the capacitor is dissipated by the concentrated resistor.

B. Experimental Results of CT-DCC

Fig. 7(a)–(d) shows in detail the voltage and current waveforms of the CT-DCC prototype during operation, where U_1 is the primary-side voltage of the coupling transformer, I_1 is the current flowing through CT-DCC, U_2 is the secondary-side voltage of the coupling transformer, and I_2 is the current flowing through the resistor. The CT-DCC prototype turned ON and OFF continuously at a specific frequency. When the duty cycle is 20%, the current is discontinuous, which is used to equal the system dissipating low surplus power. When the duty cycle is 40%, the current flowing through CT-DCC is continuous. In a single experiment, the maximum current flowing through the energy dissipation resistor is 10 kA, and the power dissipated by the CT-DCC prototype is up to 10 MW, which proves the effectiveness of the topology proposed in this letter.

V. Conclusion

A novel CT-DCC of low cost and low disturbance is proposed. Coupling transformer reduces the requirement of wall bushing, and freewheeling inductance makes the current continuous to reduce the disturbance to dc-link voltage. By analyzing the requirements of ±400 kV/1100 MW offshore wind system and characteristics of CT-DCC, the parameters of CT-DCC and the control strategy are determined. Then, the 10 kV/10 MW CT-DCC prototype is developed, and the experiment results fully prove the feasibility of the CT-DCC topology. The CT-DCC combines the advantages of the concentrated DCC and ACC, which has low cost, low disturbance, and high reliability than the existing DCC.

References

[1] W. Li, M. Zhu, P. Chao, X. Liang, and D. Xu, "Enhanced FRT and postfault recovery control for MMC-HVDC connected offshore wind farms," *IEEE Trans. Power Syst.*, vol. 35, no. 2, pp. 1606–1617, Mar. 2020.

[2] A. M. Rauf, V. Khadkikar, and M. S. El Moursi, "A new fault ride-through (FRT) topology for induction generator based wind energy conversion systems," *IEEE Trans. Power Del.*, vol. 34, no. 3, pp. 1129–1137, Jun. 2019.

[3] T. D. Vrionis, X. I. Koutiva, N. A. Vovos, and G. B. Giannakopoulos, "Control of an HVdc link connecting a wind farm to the grid for fault ride-through enhancement," *IEEE Trans. Power Syst.*, vol. 22, no. 4, pp. 2039–2047, Nov. 2007.

[4] Ł. Huchel, M. S. El Moursi, and H. H. Zeineldin, "A parallel capacitor control strategy for enhanced FRT capability of DFIG," *IEEE Trans. Sustain. Energy*, vol. 6, no. 2, pp. 303–312, Apr. 2015.

[5] L. Xu, L. Yao, and C. Sasse, "Grid integration of large DFIG-based wind farms using VSC transmission," *IEEE Trans. Power Syst.*, vol. 22, no. 3, pp. 976–984, Aug. 2007.

[6] M. Ndreko, A.-M. Bucurenciu, M. Popov, and M. A. M. M. van der Meijden, "On grid code compliance of offshore MTDC grids: Modeling and analysis," in *Proc. IEEE Eindhoven PowerTech*, Eindhoven, The Netherlands, 2015, pp. 1–6.

[7] C. Xu, X. Zhang, Z. Yu, B. Zhao, Z. Chen, and R. Zeng, "A novel DC chopper with MOV-based modular solid-state switch and concentrated dissipation resistor for ±400 kV/1100 MW offshore wind VSC-HVDC system," *IEEE Trans. Power Electron.*, vol. 35, no. 5, pp. 4483–4488, May 2020.

[8] A. M. A. Haidar, K. M. Muttaqi, and M. T. Hagh, "A coordinated control approach for DC link and rotor crowbars to improve fault ride-through of DFIG-based wind turbine," *IEEE Trans. Ind. Appl.*, vol. 53, no. 4, pp. 4073–4086, Jul./Aug. 2017.

[9] G. Ramtharan *et al.*, "Fault ride through of fully rated converter wind turbines with AC and DC transmission systems," *IET Renewable Power Gener.*, vol. 3, no. 4, pp. 426–438, Dec. 2009.

[10] C. Nentwig, J. Haubrock, R. H. Renner, and D. van Hertem, "Application of DC choppers in HVDC grids," in *Proc. IEEE Int. Energy Conf.*, Leuven, Belgium, 2016, pp. 1–5.

[11] B. Xu, C. Gao, J. Zhang, J. Yang, B. Xia, and Z. He, "A novel DC chopper topology for VSC-based offshore wind farm connection," *IEEE Trans. Power Electron.*, vol. 36, no. 3, pp. 3017–3027, Mar. 2021.